Viral-Induced Alternative Splicing of Host Genes Promotes Influenza Replication

Matthew G Thompson[1,2], Mark Dittmar[3], Michael J Mallory[2], Prasanna Bhat[4], Max B. Ferretti[2,3], Beatriz MA Fontoura[4], Sara Cherry[1,2,3] and Kristen W. Lynch[1,2]*

[1]Biochemistry and Molecular Biophysics Graduate Group and Departments of [2]Biochemistry and Biophysics and [3]Pathology, Perelman School of Medicine, University of Pennsylvania, Philadelphia, PA 19104, [4]Department of Cell Biology, UT Southwestern Medical Center, Dallas, TX 75390

Keywords: Influenza, Virus, Alternative Splicing, CLK, hnRNP K

* corresponding author E-mail: klync@pennmedicine.upenn.edu

Abstract

Viral infection induces the expression of numerous host genes that impact the outcome of infection. Here we show that infection of human lung epithelial cells with Influenza A virus (IAV) also induces a broad program of alternative splicing of host genes. While these splicing-regulated genes are not enriched for canonical regulators of viral infection, we find that many of these genes do impact replication of IAV. Moreover, specific inhibition of the IAV-induced splicing in several cases also attenuates viral infection. We further show that approximately a quarter of the IAV-induced splicing events are regulated by hnRNP K, a host protein that required for efficient splicing of the IAV M transcript in nuclear speckles. Notably, we find that hnRNP K accumulates in nuclear speckles upon IAV infection, which is likely to alter the accessibility of hnRNP K for host transcripts thereby leading to a program of host splicing changes that promote IAV replication.

Introduction

Influenza A virus (IAV) is a ubiquitous and significant health threat, resulting in 290,000 – 650,000 deaths per year worldwide ("WHO | Influenza (Seasonal)," 2019). In the United States alone, IAV is estimated to result 12,000 -56,000 deaths annually ("Estimated Influenza Illnesses, Medical Visits, Hospitalizations, and Deaths Averted by Vaccination in the United States | CDC," 2019), with an estimated $11.2 billion cost (Putri et al., 2018). While efforts are ongoing to treat the virus, there still is no universal prevention or cure. This lack of treatment is due, in part, to the virus's ability to rapidly mutate and develop resistance (Hussain et al., 2017). Therefore, it is important to further understand how IAV and host cells interact during infection in order to develop new avenues for antiviral therapies.

IAV infection results in large changes to the host gene expression landscape. Our understanding of these changes has largely been shaped through studies using microarray technology, limiting analyses to the measurement of transcript abundance. However, several recent studies have utilized advances in next generation sequencing to observe host and viral gene expression during infection in greater detail than ever before. For example, IAV infection has been shown to induce a range of gene expression phenotypes such as RNA polymerase readthrough (Bauer et al., 2018; Heinz et al., 2018; Zhao et al., 2018), translational shutoff (Bercovich-Kinori et al., 2016), altered genome architecture (Heinz et al., 2018), and targeted transcript degradation (Gaucherand et al., 2019). In addition, a recent transcriptome-wide study identified not only transcript abundance changes, but also global changes in alternative splicing isoforms (Fabozzi et al., 2018). These observations are in agreement with a growing awareness that viral

infection can not only alter gene expression but also lead to altered splicing patterns. Host splicing changes have been observed during infection with DNA viruses (HSV-1 (Hu et al., 2016), HCMV (Batra et al., 2016)) as well as RNA viruses such as reovirus (Boudreault et al., 2016), dengue virus (Sessions et al., 2013), and zika virus (Hu et al., 2017). However, these studies represent only the tip of the iceberg as they have mostly lacked the sequencing depth, and subsequent orthogonal validation, that is needed for a comprehensive quantitative analysis of host splicing (Mehmood et al., 2019; Shen et al., 2012)(Vaquero-Garcia et al., 2016). Therefore, we set out to comprehensively define the scope of host splicing changes during IAV infection in order to begin to address the underlying mechanisms and functional implications of such viral-induced alterations to the host transcriptome.

Mechanistically, changes in host splicing under any condition are generally due to regulation of RNA binding proteins that, in turn, control the host splicing machinery. Splicing factors bind at a myriad of sites throughout a nascent pre-mRNA, and influence the inclusion or exclusion of specific exons, and in some cases introns, by influencing the recruitment of spliceosomal components to splice sites (Fu and Ares, 2014). In some cases, it has been shown that that viruses directly interact with the splicing machinery to alter splice site choice. For example, dengue virus NS5 alters splicing through interaction with the U5 snRNP (De Maio et al., 2016) component of the spliceosome, and the piconaviral RdRp interacts with RNA helicase Prp8 to stall splicing (Liu et al., 2014). Viruses can also influence the localization and/or expression of splicing factors, as has been observed in poliovirus (Álvarez et al., 2013), rotavirus (Dhillon et al., 2018), alphavirus (Barnhart et al., 2013), HCV (Shwetha et al., 2015), picornavirus (Florez et al.,

2005), and HCMV (Batra et al., 2016); and the resulting change in the nuclear concentration of splicing regulatory proteins likely contributes to alternative splicing of host genes. In the case of IAV, however, it is unclear how and if viral interactions with the splicing machinery impact host splicing patterns. While it is known that the IAV protein NS1 inhibits splicing *in vitro* through interaction with the spliceosomal U6 snRNA, the relevance of this interaction in cells has not been shown (Qiu et al., 1995).

Here we demonstrate that infection of human cells with IAV induces widespread alternative splicing changes in host genes. Similar changes in splicing are not observed upon treatment with interferon, demonstrating that this program of IAV-induced splicing is a direct consequence of viral infection rather than a secondary effect of the host innate immune response. Importantly, at least 30 of the 61 genes tested that harbor IAV-induced splicing events influence IAV infection. Moreover, directly manipulating splicing of several of these transcripts confirmed that IAV-induced changes in alternative splicing have direct consequences on viral replication. Mechanistically, we found that almost 25% of the IAV-induced splicing changes are also regulated by hnRNP K, a well-known splicing regulator whose subnuclear distribution we show to be altered upon IAV infection. Previously, we demonstrated that hnRNP K promotes splicing of the IAV M segment transcript to generate the M2 protein (Mor et al., 2016; Thompson et al., 2018; Tsai et al., 2013). This suggests that the virus co-opts hnRNP K to promote infection both directly by inducing viral gene splicing, and indirectly by altering hnRNP K splicing on pro-viral transcripts altogether promoting replication. Altogether this work demonstrates the importance of alternative splicing for robust infection and replication of IAV and suggests mechanisms for how such viral-induced regulation of host splicing is achieved.

Results

Host gene expression changes are induced upon IAV A/WSN/33 infection.

As a first step toward understanding the impact of IAV infection on the transcriptome, human epithelial A549 cells were infected with IAV A/WSN/33 at a multiplicity of infection (moi) of 2, to yield ~90% infection of cells (Condit, 2013), and total RNA was isolated at 0, 6 and 12 h post infection (HPI). These experiments were performed in biological triplicate. mRNA from each replicate was poly(A)-selected and used to make cDNA libraries for 150 nucleotide, paired-end, Illumina Hi-Seq sequencing. Reads were then mapped to human and viral genomes as outlined in **Fig. 1a**. At 6 and 12 HPI, IAV RNA accounted for >30% of mapped reads (**Fig. 1b**). Despite the large percentage of reads mapping to the viral genome, 60-70 million reads, on average, were mapped to the host genome (**Supplementary Fig. 1a-b**). Importantly, this depth falls within the recommended depth (~60 million reads) for robust and reproducible splicing and differential expression analyses (Mehmood et al., 2019; Shen et al., 2012).

Differential expression analysis of host transcripts revealed 3,375 changes (log2 fold > 1, $p<0.05$) at 6 HPI and 8,185 changes at 12 HPI, with an overlap of 2,549 changes (**Fig. 1c**, list of differentially expressed genes found in **Supplementary Table S1**). Gene ontology (GO) analysis of changes at 6 HPI showed an enrichment for genes associated with host response to virus, while at 12 HPI, GO terms were enriched for categories such as DNA repair and stress (**Fig. 1d**). GO analysis of the 2,549 genes differentially expressed at both 6 and 12 HPI (**Fig. 1c**, green overlap) also showed the expected enrichment for host response to virus. We further confirmed the robust induction of individual genes that are frequently used as markers of the innate anti-viral immune

response by RT-qPCR at both 6 and 12 HPI (**Fig. 1e**). Together these data show that under the conditions of our experiment, IAV A/WSN/33 infection induces a robust host innate immune response within 6 hours. By 12 HPI we observe a further progression of infection and a corresponding stress response in the host.

Influenza A/WSN/33 infection results in differential splicing of host transcripts

Next, we quantified global changes in host splicing changes using a previously established algorithm, MAJIQ, that identifies all standard splicing events as well as complex splicing patterns (Vaquero-Garcia et al., 2016). Importantly, the detection of splicing by MAJIQ is not based on any pre-determined identification of exons, rather MAJIQ can identify any de novo pattern of splicing observed in the RNA-Seq reads (Vaquero-Garcia et al., 2016). At 6 HPI, we identified 1,162 splicing differences at 861 unique genes with a threshold for changes in percent isoform expression (ΔPSI) of greater than or equal to 10% (**Fig. 2a,b**). Using an even more stringent cut-off of 20% ΔPSI, we found 1,931 splicing changes at 12 HPI, 896 of which overlapped with those splicing events observed to vary at 6 hours (**Fig. 2a,b**; lists of all splicing changes are provided in **Supplementary Table S2**). We used a more stringent threshold at 12 HPI based on the fact that when plotting the ΔPSI values of the overlapping 896 splicing changes against each other, we see a trend in which splicing changes increase during the course of infection (**Supplementary Fig. S2a**). This trend in increased ΔPSI over time is consistent with host splicing being regulated directly in response to viral load. We have therefore focused our further analysis on the 896 splicing events that are observed at both 6 and 12 hours, as these are both the most reproducible and most correlated with virus levels.

We are particularly interested in virus-induced changes in splicing, rather than those induced as a secondary consequence of innate immune signaling. Therefore, we tested whether the splicing changes induced by IAV infection are also regulated directly by interferon. Importantly, we found that of 10 splicing events we validated in orthogonal RT-PCR assays to change splicing during viral infection, none exhibit splicing regulation upon treatment with interferon beta (IFNβ), despite the fact that this treatment induces expression of known IFNβ-target genes (**Supplemental Fig. S2b,c**). Therefore, we conclude that the majority of the changes in splicing we observed upon IAV infection are a direct consequence of viral load and not a secondary effect of interferon signaling.

The 896 infection-induced splicing events from Figure 2b are encompassed in 631 genes. Notably, only 43 of these genes also exhibit changes in abundance upon viral infection (**Fig. 2c**), consistent with many other studies that have found that genes regulated by splicing and transcription are largely distinct (Gazzara et al., 2017; Ip et al., 2007; Shinde et al., 2017). Moreover, GO analysis of the 588 genes that are differentially spliced, without changes in abundance, finds an enrichment for genes associated with RNA processing, not immune defense (**Fig. 2d**). In summary, IAV infection induces a host splicing program that is functionally distinct from the host transcriptional response.

To focus on genes that are regulated solely by splicing and not expression we have removed the 43 differentially spliced and expressed genes from our list of splicing events in the remainder of our analysis, leaving 833 distinct splicing changes in 588 genes. These 833 overlapping splicing events were then categorized by the type of alternative splicing (**Fig. 2e**). ~25% of the alternative splicing events are “classic” splicing events falling into alternative 5’ splice site, alternative 3’ splice site, and simple cassette exon

events (211 splicing changes total). We also find many events classified as either complex or uncategorized, consistent with previous studies using MAJIQ (Vaquero-Garcia et al., 2016). While interesting, these complex events are challenging to explore in terms of functional consequence or mechanism (Vaquero-Garcia et al., 2016). Therefore, we focused our subsequent studies on the more canonical splicing events.

Infection-induced splicing events encode proteins important for IAV replication

We next investigated the role of the genes harboring viral-regulated splicing events in viral infection, focusing on the 211 classic splicing events (single exon cassettes, alternative 5' splice site, and alternative 3' splice site) due to their robustness and ease of analysis by RT-PCR (**Fig. 2e**). We further filtered this set of 211 events for alternative splicing occurring within the coding sequence of transcripts, which would potentially alter the protein sequence. This resulted in a list of 61 alternatively spliced candidate genes (**Fig. 3a**). The functional importance of these 61 genes was tested using an siRNA-based screen to define which of these genes alters IAV infection when depleted. Briefly, A549 cells were transfected with siRNAs (two per gene) for 48 h, then single-cycle IAV infections were performed for 24 h and IAV infected cells were scored by staining for IAV NP protein via immunofluorescence. We also quantified cell viability and removed any candidate gene where cell viability was reduced by 25% or more after siRNA treatment. Positive "hits" in this screen were defined by genes where siRNA treatment induced a greater than 20% change in the number of IAV-positive cells in duplicate screens (**Fig. 3**). Given these parameters, we find that knock down of 25 of the 61 genes yielded a change of greater than 20% in the number of IAV-positive cells (**Fig. 3b,c**). We also

wanted to capture genes that might be important for viral particle production and subsequent re-infection rather than initial infection. Thus, for the seven genes that maintained cell viability but did not alter NP expression in our initial screen, we also carried out a multi-cycle infection assay in which we scored viral titer levels. Notably, we found that knockdown of 5 of these 7 genes resulted in dramatic (≥5.5-fold) decreases of infectious viral particles (**Fig. 3d**). Therefore, together, approximately half of the alternatively spliced genes we tested (30/61) influence the IAV infection cycle. We note that while CREB1 has previously been reported to be pro-viral (König et al., 2010), we see little impact of siRNAs of this gene in our screen (**Fig. 3c**). By contrast, our screen did replicate previous studies that found CLK1 and RAB11FIP3 to influence viral infection (Bruce et al., 2010; Karlas et al., 2010; Li et al., 2010).

Alternative splicing of host genes alters IAV replication

Having shown that many genes which are alternatively spliced during infection impact IAV replication, we next wanted to test whether the importance of these genes to infection was directly linked to splicing. In other words, in contrast to the experiments in Figure 3 in which the complete gene was targeted, we sought to test the functional impact of specifically blocking expression of the viral-induced isoform. To do so, we employed a previously established approach in which antisense morpholino oligonucleotides (AMO's) are targeted to the exon-intron boundaries of alternative exons, promoting the skipping of the targeted exons (Fiszbein et al., 2019; Mallory et al., 2011; Martinez et al., 2015). By employing this strategy, splicing events where exon usage is increased upon viral infection can be blocked. Importantly, this strategy does not impact translation of the

target mRNAs, as the AMOs only interact with the pre-mRNA. Of the 30 alternatively spliced genes shown to alter viral replication (**Fig. 3b-d**), 11 exhibited increased exon inclusion upon IAV infection. Of these 11, five were successfully modulated by AMO's: CLK1, RAB11FIP3, PPIP5K2, IQCB1, and REPIN1 (**Fig. 4a, Supplementary Fig. S3a**). We also were able to modulate CREB1 splicing (**Supplementary Fig. S3a**), which we included given the previous reports implicating this gene in IAV infection (König et al., 2010).

To assess if AMO treatment influenced IAV infection or IAV titers, A549 cells transfected with AMO's were infected with IAV at a moi of 0.01 for 48 hours. Levels of viral replication were measured by RT-qPCR assaying vRNA levels (**Fig. 4b**). In addition, infectious particles were measured via plaque assay (**Fig. 4c**). Remarkably, switching the splicing of CLK1, RAB11FIP3, and PPIP5K2 by AMO resulted in significant changes of at least 2-fold at both the titer and vRNA level (**Fig. 4b,c**) with no general toxicity to the cells (**Supplementary Fig. S3b**). In contrast, CREB1, IQCB1 and REPIN1 AMO treatment resulted in little to no changes at the viral titer or vRNA level compared to mock treatments (**Fig. 4b,c**). Given that several splicing changes occur at once during IAV infection, we also tested whether modifying multiple splicing changes simultaneously would have additive effects. Indeed, a combination AMO treatment targeting CLK1, RAB11FIP3, and PPIP5K2 splicing together, resulted in a larger decrease in viral titers compared to any of the single AMO treatments (**Fig. 4d**; ~4-fold instead of ~2-fold). These data show that direct alteration of host splicing events upon viral infection impacts viral replication, at least for a subset of genes. Even for those genes in which we do not observe a direct functional impact of viral-induced splicing (e.g. IQCB1), it is possible that

splicing regulation contributes to gene function and viral replication in a manner that is beyond the detection of our current assays.

hnRNP K regulates a subset of influenza A sensitive splicing events

We next set out to investigate how IAV infection impacts alternative splicing. We focused on the host protein hnRNP K because it was previously shown to be a pro-viral factor that regulates splicing of IAV M segment RNA (Mor et al., 2016; Thompson et al., 2018; Tsai et al., 2013). We and others have also shown that hnRNP K regulates splicing of host transcripts (Thompson et al., 2018; Venables et al., 2008). Therefore, we first tested if hnRNP K is important for IAV replication independent of its regulation of M segment splicing. In previous work, we generated an IAV mutant strain in which hnRNP K cannot bind to the M segment to regulate splicing (ΔK-mut; (Thompson et al., 2018). To determine if hnRNP K regulates IAV replication in the context of this virus, we depleted hnRNP K in A549 cells using siRNAs and assayed infectious virus particles 48 hours post-infection. Importantly, we show that while the ΔK-mut IAV M2 splicing is no longer sensitive to hnRNP K levels (**Supplementary Fig. 4a,b**), viral propagation is still attenuated upon hnRNP K knockdown (**Fig. 5a**). These data indicate that hnRNP K is required for IAV replication independent of its role in M splicing.

To determine if any of the IAV-sensitive alternative splicing events are dependent on hnRNP K, we depleted hnRNP K in A549 cells by stably expressing a doxycycline-inducible shRNA (**Fig. 5b**). Splicing changes that occur in response to hnRNP K knockdown were quantified using MAJIQ, filtering for significant changes of 10% or more in percent splicing (ΔPSI). In agreement with previous studies, we observe large changes

in host splicing upon hnRNP K depletion (**Supplementary Table S2**)(Thompson et al., 2018; Venables et al., 2008). Importantly, 21% of the influenza-induced splicing changes are also hnRNP K-responsive (**Fig. 5c**). To determine if hnRNP K positively or negatively regulates splicing of the IAV-dependent splicing events, we plotted the impact of hnRNP K and IAV infection on PSI values of the 179 common splicing events (**Fig. 5d**). We find 65% of splicing changes are regulated similarly by hnRNP K depletion and IAV infection, whereas for the remainder, hnRNP K depletion has the opposite effect of infection. We validated many of these splicing changes in response to both IAV infection and hnRNP K knockdown by RT-PCR, including both those that exhibit a similar and an opposite change under these two conditions (**Fig. 4a, Supplementary Fig. 2b**). The observed high validation rates are consistent with previous studies with MAJIQ (Vaquero-Garcia et al., 2016).

hnRNP K nuclear distribution is altered during infection

Based on the two populations of hnRNP K and IAV-responsive splicing events, we propose at least two models for how hnRNP K-dependent splicing is regulated during infection. The abundance of splicing events for which hnRNP K depletion phenocopies infection at the splicing level suggests that hnRNP K may be functionally depleted or inhibited during infection. By contrast, for events with opposite ΔPSI values between hnRNP K depletion and infection, hnRNP K activity may be enhanced by a co-factor that is increased or activated upon infection. Both of these models imply a change to hnRNP K activity upon infection. However, western blot analysis revealed little to no differences in hnRNP K expression or nucleocytoplasmic localization. (**Fig. 6a**). Analyses of hnRNP

K phosphorylation via phos-tag SDS-PAGE showed no reproducible changes overall, although we do note a minor increase in phosphorylation, particularly in the nuclear fraction (**Fig. 6a**). These results are in agreement with previous mass spectrometry-based studies showing that total hnRNP K level and phosphorylation do not significantly change during IAV infection (Coombs et al., 2010; Dapat et al., 2014).

Although hnRNP K levels did not appear to change between the cytoplasm and nucleus, it is possible more subtle changes in hnRNP K sub-cellular localization occur during infection. In past work we showed that hnRNP K activates IAV M RNA splicing within nuclear speckles, as opposed to the nucleoplasm where most splicing of host transcripts is thought to occur (Mor et al., 2016; Thompson et al., 2018). Therefore, we asked if the speckle-associated pool of hnRNP K is altered during IAV infection. To test this, hnRNP K colocalization with nuclear speckle associated protein, SC35, was measured using fluorescence microscopy in mock and IAV infected A549 cells (**Fig. 6b-c**). Strikingly, we observed that hnRNP K levels at nuclear speckles significantly increase during IAV infection (**Fig. 6d**). Therefore, we propose that at least one of the mechanisms by which IAV results in alterations in hnRNP K-regulated splicing events is through enhanced recruitment of hnRNP K to nuclear speckles. Such re-localization effectively depletes hnRNP K from co-transcriptional splicing processes in the nucleoplasm, and potentially enhances hnRNP K activity on splicing events that occur at nuclear speckles, including the IAV M transcript.

Discussion

Previous studies have established that the host transcriptome is profoundly altered upon IAV infection. While much of this work has shown that regulation of host transcription is a major component of these changes, only recently have post-transcriptional events, such as alternative splicing, begun to be analyzed (Fabozzi et al., 2018). Here we identify a program of host splicing that is regulated by IAV infection, and show that many of these splicing changes occur within genes that promote IAV replication. Furthermore, directly manipulating a subset of these IAV-induced splicing changes, using splice-blocking AMO's, also attenuates infection. Together these data implicate infection-induced changes in host splicing as a previously unrecognized mechanism by which viruses promote infection.

Our RNA-seq analyses of A/WSN/33 infected A549 cells revealed functionally distinct categories of genes that are regulated by transcriptional and splicing responses. Genes that exhibit differential expression are enriched for genes involved in immune response and viral defense, consistent with previous studies (Fabozzi et al., 2018; Ioannidis et al., 2012). By contrast, GO analyses of genes that harbor splicing changes demonstrates enrichment for RNA processing categories. Moreover, we observe very little overlap between the genes that are differentially spliced versus those that show differential expression. These data suggest that the host splicing response to virus is functionally distinct from the transcriptional response. We are unable to directly compare our data to other RNA-Seq studies due to differential experimental design and depth of sequence; however, our findings are generally consistent with the prediction that IAV infection induces changes in host splicing in addition to, and separate from, changes in

transcription. Patterns similar to this have been observed in other systems. For example, T-cell stimulation results in robust transcriptional and splicing changes, however very little overlap is observed between the categories (Martinez et al., 2012).

Our analyses of host splicing changes adds to a pattern of IAV inducing a variety transcriptomic phenotypes. Recent studies observing altered genome architecture, transcript 3' end defects, and PA-X targeted transcript degradation during infection all have links to splicing (Gaucherand et al., 2019; Heinz et al., 2018; Zhao et al., 2018). One observation was that of transgenic, defective, and unannotated splicing in relation to transcription termination (Heinz et al., 2018; Zhao et al., 2018). While our splicing analyses did not account for these specific splicing types, we would predict for them to be present in our experiments to some extent. Importantly, the alternatively spliced transcripts we describe here are not products of defective or transgenic splicing, and are likely not induced by the same transcription defects described in other studies. Additionally, the IAV endonuclease PA-X was shown to preferentially target spliced transcripts (Gaucherand et al., 2019). However the alternatively spliced genes we define here do not overlap with PA-X targeted genes (Gaucherand et al., 2019). Therefore, while splicing appears to contribute to many facets of IAV-induced transcriptome changes, we propose that a portion of the functional splicing events described here are independent of previously described mechanisms.

Although the set of genes that we identify to undergo alternative splicing upon IAV infection are not enriched for known regulators of viral replication, we demonstrate that half of the splicing-regulated genes we tested (30/61) do impact IAV infection or propagation. This includes genes involved in cell signaling, intracellular trafficking and

gene expression. In addition to demonstrating that many of the host genes that undergo IAV-induced splicing changes are involved in controlling infection, in several cases we directly show that changing the splicing of these genes alters IAV replication (**Fig. 4**). For example, IAV infection induces inclusion of alternative CLK1 exon 4, which results in expression of the canonical full-length isoform of the protein (**Fig. 4a**). By contrast, skipping of exon 4 is observed in uninfected cells and introduces an early stop codon that truncates the kinase domain of protein (Duncan et al., 1997; Uzor et al., 2018). Therefore, in the case of CLK1, both the AMO that blocks exon 4 inclusion (**Fig. 4**), and the siRNA (**Fig. 3**), are expected to decrease the expression of active protein. Given that previous studies have established CLK1 to be required for efficient IAV replication (Artarini et al., 2019; Karlas et al., 2010; Zu et al., 2015), our data is consistent with a model in which IAV infection promotes exon inclusion to increase production of full-length functional CLK1 kinase that, in turn, promotes viral growth.

For RAB11FIP3, IAV induces the inclusion of a non-canonical in-frame alternative exon (**Fig. 4a**), resulting in expression of an alternate isoform of this protein. The function of the additional protein sequence remains unclear, as it lies upstream of the defined RAB11 binding domain (Shiba et al., 2006) and does not contain known phosphorylation sites (Collins et al., 2012). Regardless, this non-canonical isoform appears to promote IAV infection, as blocking the variable exon up-regulates the canonical isoform and limits IAV replication in multi-cycle infections (**Fig. 4b**). Interestingly, a previously established model suggests that RAB11FIP3 may compete with IAV vRNPs for RAB11 on endosomes in the particle assembly pathway (Vale-Costa et al., 2016). Therefore, it is possible that the canonical RAB11FIP3 isoforms may interfere with particle assembly,

such that it is beneficial to the virus for this canonical isoform to be decreased through splicing.

PPIP5K2 exon inclusion is also increased upon viral infection, producing increased levels of the canonical full-length isoform of the RNA (**Fig. 4a**). By contrast, forced skipping of this exon results in decreases in viral titers and vRNA (**Fig 4a-c**). Interestingly, PPIP5K2 has been previously thought to limit to influenza A replication (Pulloor et al., 2014), as it was shown that catalytic activity of PPIP5K2 is required for efficient IFNβ production, and in turn, that knockdown of PPIP5K2 resulted in viral load increases. The exon that is skipped in uninfected cells removes a portion of peptide sequence without altering the downstream reading frame. It is possible that the resultant smaller protein has increased catalytic activity, perhaps through removal of an inhibitory interaction, such that altering the splicing of PPIP5K2 may reduce PPIP5K2 function.

Importantly, we show a previously established pro-viral host factor, hnRNP K, regulates a subset of the splicing events that change in response to IAV infection, including CLK1, RAB11FIP3 and PPIP5K2. Notably, hnRNP K undergoes increased sequestration into nuclear speckles upon viral infection, suggesting that this may functionally deplete this protein from host genes that are typically spliced outside of speckles. HnRNP K was previously established to be important for IAV M segment splicing regulation (Mor et al., 2016; Thompson et al., 2018; Tsai et al., 2013). However, IAV replication is sensitive to hnRNP K expression even in the context of a mutant IAV in which hnRNP K is not required for M segment splicing regulation, consistent with hnRNP K regulating important pro-viral splicing events in host genes (**Fig. 5a, Supplementary Fig. S4a,b**). It is possible, however, that hnRNP K is also important for additional viral

processes such as regulating transcription or translation of viral transcripts, as hnRNP K has been implicated to regulate many facets of RNA processing other than splicing (Bomsztyk et al., 2004). Nonetheless, given that hnRNP K levels regulate 21% of detected IAV-induced splicing changes (**Fig. 5c**), many of which encode for proteins that influence viral replication (**Fig. 3c**), we contend that hnRNP K regulation of host transcript splicing is an important process during IAV infection.

While our data clearly shows changes in host splicing upon IAV infection (**Fig. 2**), many of which are regulated by host splicing factor hnRNP K (**Fig. 5c**), it is not clear if these splicing changes are induced through host or viral mechanisms. A virus-centric model would suggest that viral manipulation of host splicing-related pathways causes the splicing changes observed during infection. By contrast, a host-centric model would predict the splicing changes observed during infection are part of a host response to pathogen. Likely, the changes we observe here are a mixture of both models. However, RT-PCR analysis of a panel of IAV-sensitive splicing events in the context of IFNβ treatment identified no significant splicing changes, thus ruling out a model in which splicing changes are primarily triggered indirectly by interferon secretion, as a secondary consequence of the innate immune response.

In sum, we demonstrate here a feedback loop between viral-induced regulation of splicing of host genes and subsequent viral infection. This is yet another example of the intricate competition between host and virus, involving multiple layers of regulation and counter-regulation[53,54]. We also demonstrate one of the mechanisms driving this IAV-induced regulation of splicing. Future studies will be required to further uncover additional

underlying mechanisms by which IAV control host splicing, and to determine if manipulation of these mechanisms has potential for anti-viral therapeutic intervention.

Methods

Cell culture and Viruses

Human lung adenocarcinoma epithelial cells (A549) were cultured in RPMI 1640 (Corning: 10-040-CV), 10% heat-inactivated FBS (Gibco: 16000-044), and 100 units ml−1 Pen/Strep antibiotics. MDCK cells were cultured in high-glucose DMEM (Corning: 10-013-CV), 10% heat-inactivated FBS (Gibco) and 100 units ml−1 Pen/Strep antibiotics. All cells were maintained at 37 °C with 5% CO_2. Cells were tested negative for mycoplasma. Cell lines were obtained and authenticated by ATCC (A549: CCL-185, MDCK: PTA-6500). A/Puerto Rico/8/1934 (PR8) and A/WSN/33 (WSN) strains were used as specified for individual experiments. ΔK-mut virus was generated as previously described in another study (Thompson et al., 2018). Viral titers were determined via plaque assay in MDCK cells as the average to technical replicates.

Infections

For infections, A549 cells were grown to 80% confluency, washed with PBS, and inoculated with viral titer diluted in PBS•BA (DPBS with Ca and Mg (Corning: 21-031-CV), 0.2% BSA (Lampire: 7500810), and 100 units ml−1 Pen/Strep antibiotics) for 1 h at room temperature (22˚C). Cells were then washed with PBS and incubated in Infection media (1X MEM, 0.2% BSA, 10 mM HEPES buffer, 0.12% $NaHCO_3$, 100 units ml−1 Pen/Strep antibiotics) at 37˚C with 5% CO_2 until desired time-point. At time-points, media was collected for plaque assay analyses. For protein and RNA analyses, wells were rinsed with PBS and either pelleted and lysed with RIPA buffer for Western blot analysis or RNA was extracted using RNA-Bee (amsbio: CS-501B).

Plaque assays

MDCK cells were grown to 100% confluency in 12-well plates. Viral titers to be assayed were serially diluted in PBS•BA (DPBS with Ca and Mg (Corning: 21-031-CV), 0.2% BSA (Lampire: 7500810), and 100 units ml−1 Pen/Strep antibiotics). MDCK cells were then washed in PBS and viral dilutions were added to each well and left to inoculate for 1 h at room temperature (22˚C). Viral dilutions were then removed and 1 ml of plaque overlay media was added to each well (1X MEM, 0.2% BSA, 10 mM HEPES buffer, 0.22% $NaHCO_3$, 0.01% DEAE Dextran, 100 units ml−1 Pen/Strep antibiotics, and 0.6% Agar (Oxoid). Plates were stored upside-down at 37˚C with 5% CO_2 for 48 h at which point cells were fixed with 3.6% formaldehyde. Gel plugs were then removed, cells were stained with Crystal violet, and plaques were counted.

Depletion of hnRNP K from A549 cells.

For knockdown of hnRNP K to test viral replication (Fig. 5a), A549 cells were treated with 50 nM siRNA (Dharmacon, SMARTpool, M-011692-00) as previously described (Thompson et al., 2018). For RNA-Seq and validation experiments, hnRNP K was stably depleted from A549 cells using a lentiviral expressed doxycycline-inducible shRNA with sequence:

agcgGGACCTATTATTACTACACAATAGTGAAGCCACAGATGTATTGTGTAGTAATAA TAGGTCC (target underlined) This shRNA vector and its use are described in detail previously (Martinez et al., 2015).

RNA-seq of infected or hnRNP K knockdown cells

For infections A549 cells were grown to 80% confluency in 15 cm plates and infected with WSN IAV at moi = 2. At the 0, 6, and 12 h post infection, total RNA was extracted from cells. For hnRNP K knockdowns, either stable shRNA expressing or WT A549 cells were grown to 90% confluency in 15 cm plates over a span of 48 h in the presence of doxycycline. At 48 h total RNA was extracted. RNA was then DNase treated and further purified using RNeasy mini kit (Qiagen). RNA quality assessed for quality using a Nanodrop and Agilent 2100 Bioanalyzer. Samples were required to have a 260/280 ratio of >1.8 as well as a RIN value of >6 to be used for library preparation. Poly(A) selected cDNA libraries were generated on site at the University of Iowa sequencing core using standard methods. cDNA libraries were then sequenced for paired-end, 150-nt, reads on an Illumina HiSeq 4000. RNA-Seq data is accessible in GEO under study GSE142499.

RNA-seq mapping, differential expression analysis

Raw reads were aligned to the human or viral WSN genome using STAR (Dobin et al., 2013). Differential gene expression of host transcripts was performed using the R-package, DESeq2 (Love et al., 2014). Significantly changing genes were defined as those with a log2 fold-change greater than |1| and a corresponding p-value <0.05.

Splicing analysis

Spicing analyses was performed using MAJIQ (ver. 1.1.3a) as described previously (Vaquero-Garcia et al., 2016). Initial splicing analyses of 0 HPI, 6 HPI, 12 HPI, mock dox-treatment, and sh-hnRNP K samples were performed in parallel using MAJIQ builder with

default settings. ΔPSI values were quantified with the MAJIQ package, VOILA, using the following settings. 6 HPI samples were quantified against 0 HPI set at a threshold of 10. 12 HPI samples were quantified against 0 HPI set at a threshold of 20. sh-hnRNP K samples were quantified against mock dox-treated samples at a threshold of 10. Significant splicing events were those with probability values > 0.95 and a ΔPSI value greater than 10 (for 6 HPI and sh-hnRNP K) or 20 (for 12 HPI).

siRNA screen

The siRNA screen was done as previously described (Panda and Cherry, 2015). In brief, siRNA libraries targeting each gene were ordered from Ambion and aliquoted into 384-well plates. siRNAs were then transfected into 2,000 A549 cells in each well using 0.5 µl HiPerFect (Qiagen) in a total volume of 50 µl and a final concentration of 20 nM siRNA. siRNA treatment proceeded for 72 h. siRNA transfection efficiency was monitored using the siDeath control RNA. Cells were then infected with IAV PR8 at an moi of 0.1 or 0.5 for 24 h. After infections cells were fixed with 4% formaldehyde, washed twice with phosphate-buffered saline (PBS), blocked for 1 h in blocking solution consisting of PBS containing 2% bovine serum albumin (BSA), 0.1% Triton X-100, and 0.02% sodium azide, and stained with mouse anti-IAV NP primary antibody at a 1:2000 dilution in blocking solution overnight at 4 °C. The primary antibody was then replaced with blocking solution containing 5 µg/mL bisBenzimide H 33342 trihydrochloride (Sigma-Aldrich, B2261) and goat anti-mouse Alexa Fluor 488 secondary antibody (Invitrogen, A11029) at a 1:1000 dilution and incubated for 1 h at room temperature. The cells were then washed three times with PBS containing 0.1% Triton X-100 before imaging. Imaging of cells was

performed using an ImageXpress autoscope and MetaXpress software. 4 images were collected per well and a median % IAV cell score was calculated. Changes in % IAV positive cells were calculated relative to wells treated with siControl siRNA. Final values were determined as an average % change in IAV positive cells across duplicate experiments.

Antisense morpholino oligonucleotide treatment and infections

For each AMO treatment, 500,000 A549 cells were electroporated with a total of 5 nmoles AMO using a Bio-Rad Gene Pulser Xcell (settings used were default A549 cell program). AMO sequences are detailed in Supplemental Table S3. Electroporations were performed in RPMI media without FBS or antibiotics. 200,000 treated cells were seeded into 6-well plates and allowed to grow for 48 h. Splice-blocking activity each AMO at 48 h was validated using radio-labeled RT-PCR (**Fig. 4a**, **Supplementary Fig. 5a**). Cells were then infected with WSN IAV at the specified moi and time-course. At the specified time points media was collected for downstream plaque assays and total RNA was collected for further experiments.

Microscopy and quantification of subnuclear localization of hnRNP K

For subnuclear localization of hnRNP K, immunofluorescence was performed as previously described (25) using SC35 (ab11826, Abcam), hnRNP K (GTX101786, Genetex) and anti-influenza A virion polyclonal antibodies (B65141G, Meridian Life Science). For quantification of hnRNP K localization, images were captured as previously described (25). AutoQuant software was used to deconvolve z stack images.

Deconvolved images were used for surface generation and quantification using Imaris (Bitplane) software. Surface was generated for nuclear speckles using the SC35 channel. Display minimum and maximum values were adjusted to distinguish SC35 at nuclear speckles from the nucleoplasm pool. Display minimum and maximum values were kept constant for all images. DAPI channel was used for generating the nuclear surface. Threshold was adjusted manually during surface generation. Number of voxels above 10 was used as filter. Intensity sum of hnRNPK from nuclear speckle surface and nucleus surface was quantified using the Imaris software. Statistical analysis was done using an unpaired, two-tailed, t-test with Welch's correction was performed.

Interferon treatment

A549 cells were grown 80% confluency in 10 cm plates. At time of interferon treatment, fresh, pre-warmed media containing 10 ng/ml beta-interferon (STEMCELL Technologies, Cat #78113) was added to cells. Total cellular RNA was harvested 12 h post treatment using RNA-Bee (amsbio: CS-501B). IFIT1 expression was assessed via qPCR (**Supplementary Figure 2**) to validate innate immune stimulation.

qPCR analyses

cDNA was produced in a 24 µl reaction using 500 ng total cellular RNA, 1 ng of gene-specific reverse primer, and MMLV reverse transcriptase enzyme. 3 µl of cDNA was added to 10 µl qPCR reactions containing 0.5 µM forward and reverse primers as well as 1X PowerUP SYBR green master mix (ThermoFisher) in 384-well plates. Expression levels of targeted genes were calculated relative to GAPDH. qPCR primers are detailed

in Supplemental Table S3. All qPCR data is from triplicate biologic replicates, each analyzed in technical duplicate.

RT-PCR analyses

RT-PCR was carried out as described in detail previously (Martinez et al., 2015; Thompson et al., 2018). RT-PCR primers are detailed in Supplemental Table S3. All RT-PCR data is from analysis of triplicate biologic replicates.

Acknowledgements

We thank members of the Lynch, Cherry and Fontoura laboratories for helpful comments throughout this study. The NS1 antibody was a gift from Dr. Adolfo Garcia-Sastre. This work was funded by NIH grants R01 AI125524 to KWL and BMAF and R35 GM118048 to KWL. SC was supported by grants from the NIH (R01AI150246, R01AI122749, R01AI140539) and is a recipient of the Burroughs Wellcome Investigators in the Pathogenesis of Infectious Disease Award.

Contributions

MD carried out the siRNA viral infection screen, MJM generated shRNA knockdown cells and RNAs for RNA-Seq and carried out many of the Western blots, PB performed the immunofluorescence and analysis of hnRNP K localization, MBF did the interferon studies, MGT directed the overall project, together with BMAF, SC and KWL, and carried out all of the experiments not specified above. MGT and KWL wrote the manuscript with assistance from all the authors.

Competing interests

The authors declare no competing interests.

References:

Álvarez E, Castelló A, Carrasco L, Izquierdo JM. 2013. Poliovirus 2A Protease Triggers a Selective Nucleo-Cytoplasmic Redistribution of Splicing Factors to Regulate Alternative Pre-mRNA Splicing. *PLoS One* **8**:e73723. doi:10.1371/journal.pone.0073723

Artarini A, Meyer M, Shin YJ, Huber K, Hilz N, Bracher F, Eros D, Orfi L, Keri G, Goedert S, Neuenschwander M, von Kries J, Domovich-Eisenberg Y, Dekel N, Szabadkai I, Lebendiker M, Horváth Z, Danieli T, Livnah O, Moncorgé O, Frise R, Barclay W, Meyer TF, Karlas A. 2019. Regulation of influenza a virus mRNA splicing by CLK1. *Antiviral Res* **168**:187–196. doi:10.1016/j.antiviral.2019.06.003

Barnhart MD, Moon SL, Emch AW, Wilusz CJ, Wilusz J. 2013. Changes in Cellular mRNA Stability, Splicing, and Polyadenylation through HuR Protein Sequestration by a Cytoplasmic RNA Virus. doi:10.1016/j.celrep.2013.10.012

Batra R, Stark TJ, Clark E, Belzile J-P, Wheeler EC, Yee BA, Huang H, Gelboin-Burkhart C, Huelga SC, Aigner S, Roberts BT, Bos TJ, Sathe S, Donohue JP, Rigo F, Ares M, Spector DH, Yeo GW. 2016. RNA-binding protein CPEB1 remodels host and viral RNA landscapes. *Nat Struct Mol Biol* **23**:1101–1110. doi:10.1038/nsmb.3310

Bauer DLV, Tellier M, Martínez-Alonso M, Nojima T, Proudfoot NJ, Murphy S, Fodor E. 2018. Influenza Virus Mounts a Two-Pronged Attack on Host RNA Polymerase II Transcription. *Cell Rep* **23**:2119-2129.e3. doi:10.1016/j.celrep.2018.04.047

Bercovich-Kinori A, Tai J, Gelbart IA, Shitrit A, Ben-Moshe S, Drori Y, Itzkovitz S, Mandelboim M, Stern-Ginossar N. 2016. A systematic view on influenza induced

host shutoff. *Elife* **5**. doi:10.7554/eLife.18311

Bomsztyk K, Denisenko O, Ostrowski J. 2004. hnRNP K: one protein multiple processes. *Bioessays* **26**:629–38. doi:10.1002/bies.20048

Boudreault S, Martenon-Brodeur C, Caron M, Garant J-M, Tremblay M-P, Armero VES, Durand M, Lapointe E, Thibault P, Tremblay-Létourneau M, Perreault J-P, Scott MS, Lemay G, Bisaillon M. 2016. Global Profiling of the Cellular Alternative RNA Splicing Landscape during Virus-Host Interactions. *PLoS One* **11**:e0161914. doi:10.1371/journal.pone.0161914

Bruce EA, Digard P, Stuart AD. 2010. The Rab11 pathway is required for influenza A virus budding and filament formation. *J Virol* **84**:5848–59. doi:10.1128/JVI.00307-10

Collins LL, Simon G, Matheson J, Wu C, Miller MC, Otani T, Yu X, Hayashi S, Prekeris R, Gould GW. 2012. Rab11-FIP3 is a cell cycle-regulated phosphoprotein. *BMC Cell Biol* **13**:4. doi:10.1186/1471-2121-13-4

Condit RC. 2013. Principles of VirologyFields Virology, 6th Ed. Lippincott Williams and Wilkins, Philadelphia, PA. pp. 21–51.

Coombs KM, Berard A, Xu W, Krokhin O, Meng X, Cortens JP, Kobasa D, Wilkins J, Brown EG. 2010. Quantitative proteomic analyses of influenza virus-infected cultured human lung cells. *J Virol* **84**:10888–906. doi:10.1128/JVI.00431-10

Dapat C, Saito R, Suzuki H, Horigome T. 2014. Quantitative phosphoproteomic analysis of host responses in human lung epithelial (A549) cells during influenza virus infection. *Virus Res* **179**:53–63. doi:10.1016/J.VIRUSRES.2013.11.012

De Maio FA, Risso G, Iglesias NG, Shah P, Pozzi B, Gebhard LG, Mammi P, Mancini E,

Yanovsky MJ, Andino R, Krogan N, Srebrow A, Gamarnik A V. 2016. The Dengue Virus NS5 Protein Intrudes in the Cellular Spliceosome and Modulates Splicing. *PLOS Pathog* **12**:e1005841. doi:10.1371/journal.ppat.1005841

Dhillon P, Tandra VN, Chorghade SG, Namsa ND, Sahoo L, Rao CD. 2018. Cytoplasmic Relocalization and Colocalization with Viroplasms of Host Cell Proteins, and Their Role in Rotavirus Infection. *J Virol* **92**:e00612-18. doi:10.1128/JVI.00612-18

Dobin A, Davis CA, Schlesinger F, Drenkow J, Zaleski C, Jha S, Batut P, Chaisson M, Gingeras TR. 2013. STAR: ultrafast universal RNA-seq aligner. *Bioinformatics* **29**:15–21. doi:10.1093/bioinformatics/bts635

Duncan PI, Stojdl DF, Marius RM, Bell JC. 1997. In vivo regulation of alternative pre-mRNA splicing by the Clk1 protein kinase. *Mol Cell Biol* **17**:5996–6001. doi:10.1128/MCB.17.10.5996

Estimated Influenza Illnesses, Medical Visits, Hospitalizations, and Deaths Averted by Vaccination in the United States | CDC. 2019. . *CDC*. https://www.cdc.gov/flu/about/disease/2015-16.htm

Fabozzi G, Oler AJ, Liu P, Chen Y, Mindaye S, Dolan MA, Kenney H, Gucek M, Zhu J, Rabin RL, Subbarao K. 2018. Strand-specific Dual RNA-seq of Bronchial Epithelial cells Infected with Influenza A/H3N2 Viruses Reveals Splicing of Gene Segment 6 and Novel Host-Virus Interactions. *J Virol* JVI.00518-18. doi:10.1128/JVI.00518-18

Fiszbein A, Krick KS, Begg BE, Burge Correspondence CB, Burge CB. 2019. Exon-Mediated Activation of Transcription Starts Article Exon-Mediated Activation of Transcription Starts. *Cell* **179**. doi:10.1016/j.cell.2019.11.002

Florez PM, Sessions OM, Wagner EJ, Gromeier M, Garcia-Blanco MA. 2005. The Polypyrimidine Tract Binding Protein Is Required for Efficient Picornavirus Gene Expression and Propagation. *J Virol* **79**:6172–6179. doi:10.1128/jvi.79.10.6172-6179.2005

Fu X-D, Ares M. 2014. Context-dependent control of alternative splicing by RNA-binding proteins. *Nat Rev Genet* **15**:689–701. doi:10.1038/nrg3778

Gaucherand L, Porter BK, Levene RE, Price EL, Schmaling SK, Rycroft CH, Kevorkian Y, McCormick C, Khaperskyy DA, Gaglia MM. 2019. The Influenza A Virus Endoribonuclease PA-X Usurps Host mRNA Processing Machinery to Limit Host Gene Expression. *Cell Rep* **27**:776-792.e7. doi:10.1016/j.celrep.2019.03.063

Gazzara MR, Mallory MJ, Roytenberg R, Lindberg JP, Jha A, Lynch KW, Barash Y. 2017. Ancient antagonism between CELF and RBFOX families tunes mRNA splicing outcomes. *Genome Res* **27**:1360–1370. doi:10.1101/gr.220517.117

Heinz S, Texari L, Hayes MGB, Urbanowski M, Chang MW, Givarkes N, Rialdi A, White KM, Albrecht RA, Pache L, Marazzi I, García-Sastre A, Shaw ML, Benner C. 2018. Transcription Elongation Can Affect Genome 3D Structure. *Cell* **174**:1522-1536.e22. doi:10.1016/j.cell.2018.07.047

Hu B, Huo Y, Yang L, Chen G, Luo M, Yang J, Zhou J. 2017. ZIKV infection effects changes in gene splicing, isoform composition and lncRNA expression in human neural progenitor cells. *Virol J* **14**:217. doi:10.1186/s12985-017-0882-6

Hu B, Li X, Huo Y, Yu Y, Zhang Q, Chen G, Zhang Y, Fraser NW, Wu D, Zhou J. 2016. Cellular responses to HSV-1 infection are linked to specific types of alterations in the host transcriptome. *Sci Rep* **6**:28075. doi:10.1038/srep28075

Hussain M, Galvin H, Haw TY, Nutsford A, Husain M. 2017. Drug resistance in influenza A virus: the epidemiology and management. *Infect Drug Resist* **Volume 10**:121–134. doi:10.2147/IDR.S105473

Ioannidis I, McNally B, Willette M, Peeples ME, Chaussabel D, Durbin JE, Ramilo O, Mejias A, Flaño E. 2012. Plasticity and virus specificity of the airway epithelial cell immune response during respiratory virus infection. *J Virol* **86**:5422–36. doi:10.1128/JVI.06757-11

Ip JY, Tong A, Pan Q, Topp JD, Blencowe BJ, Lynch KW. 2007. Global analysis of alternative splicing during T-cell activation. *RNA* **13**:563–572. doi:10.1261/rna.457207

Karlas A, Machuy N, Shin Y, Pleissner K-P, Artarini A, Heuer D, Becker D, Khalil H, Ogilvie LA, Hess S, Mäurer AP, Müller E, Wolff T, Rudel T, Meyer TF. 2010. Genome-wide RNAi screen identifies human host factors crucial for influenza virus replication. *Nature* **463**:818–22. doi:10.1038/nature08760

König R, Stertz S, Zhou Y, Inoue A, Hoffmann HH, Bhattacharyya S, Alamares JG, Tscherne DM, Ortigoza MB, Liang Y, Gao Q, Andrews SE, Bandyopadhyay S, De Jesus P, Tu BP, Pache L, Shih C, Orth A, Bonamy G, Miraglia L, Ideker T, García-Sastre A, Young JAT, Palese P, Shaw ML, Chanda SK. 2010. Human host factors required for influenza virus replication. *Nature* **463**:813–817. doi:10.1038/nature08699

Li W, Sun W, Liu L, Yang F, Li Y, Chen Y, Fang J, Zhang W, Wu J, Zhu Y. 2010. IL-32: a host proinflammatory factor against influenza viral replication is upregulated by aberrant epigenetic modifications during influenza A virus infection. *J Immunol*

185:5056–65. doi:10.4049/jimmunol.0902667

Liu Y-C, Kuo R-L, Lin J-Y, Huang P-N, Huang Y, Liu H, Arnold JJ, Chen S-J, Wang RY-L, Cameron CE, Shih S-R. 2014. Cytoplasmic viral RNA-dependent RNA polymerase disrupts the intracellular splicing machinery by entering the nucleus and interfering with Prp8. *PLoS Pathog* **10**:e1004199. doi:10.1371/journal.ppat.1004199

Love MI, Huber W, Anders S. 2014. Moderated estimation of fold change and dispersion for RNA-seq data with DESeq2. *Genome Biol* **15**:550. doi:10.1186/s13059-014-0550-8

Mallory MJ, Jackson J, Weber B, Chi A, Heyd F, Lynch KW. 2011. Signal- and development-dependent alternative splicing of LEF1 in T cells is controlled by CELF2. *Mol Cell Biol* **31**:2184–2195. doi:10.1128/MCB.05170-11

Martinez NM, Agosto L, Qiu J, Mallory MJ, Gazzara MR, Barash Y, Fu X-D, Lynch KW. 2015. Widespread JNK-dependent alternative splicing induces a positive feedback loop through CELF2-mediated regulation of MKK7 during T-cell activation. *Genes Dev* **29**:2054–66. doi:10.1101/gad.267245.115

Martinez NM, Pan Q, Cole BS, Yarosh C a., Babcock G a., Heyd F, Zhu W, Ajith S, Blencowe BJ, Lynch KW. 2012. Alternative splicing networks regulated by signaling in human T cells. *Rna* **18**:1029–1040. doi:10.1261/rna.032243.112

Mehmood A, Laiho A, Venäläinen MS, McGlinchey AJ, Wang N, Elo LL. 2019. Systematic evaluation of differential splicing tools for RNA-seq studies. *Brief Bioinform*. doi:10.1093/bib/bbz126

Mor A, White A, Zhang K, Thompson M, Esparza M, Muñoz-Moreno R, Koide K, Lynch

KW, García-Sastre A, Fontoura BMA. 2016. Influenza virus mRNA trafficking through host nuclear speckles. *Nat Microbiol* **1**:16069. doi:10.1038/nmicrobiol.2016.69

Panda D, Cherry S. 2015. A genome-wide RNAi screening method to discover novel genes involved in virus infection. *Methods* **91**:75–81. doi:10.1016/J.YMETH.2015.07.002

Pulloor NK, Nair S, Kostic AD, Bist P, Weaver JD, Riley AM, Tyagi R, Uchil PD, York JD, Snyder SH, García-Sastre A, Potter BVL, Lin R, Shears SB, Xavier RJ, Krishnan MN. 2014. Human Genome-Wide RNAi Screen Identifies an Essential Role for Inositol Pyrophosphates in Type-I Interferon Response. *PLoS Pathog* **10**:e1003981. doi:10.1371/journal.ppat.1003981

Putri WCWS, Muscatello DJ, Stockwell MS, Newall AT. 2018. Economic burden of seasonal influenza in the United States. *Vaccine* **36**:3960–3966. doi:10.1016/J.VACCINE.2018.05.057

Qiu Y, Nemeroff M, Krug R. 1995. The influenza virus NS1 protein binds to a specific region in human U6 snRNA and inhibits U6-U2 and U6-U4 snRNA interactions during splicing. RNA. *Rna*.

Sessions OM, Tan Y, Goh KC, Liu Y, Tan P, Rozen S, Ooi EE. 2013. Host Cell Transcriptome Profile during Wild-Type and Attenuated Dengue Virus Infection. *PLoS Negl Trop Dis* **7**:1–12. doi:10.1371/journal.pntd.0002107

Shen S, Park JW, Huang J, Dittmar KA, Lu Z, Zhou Q, Carstens RP, Xing Y. 2012. MATS: a Bayesian framework for flexible detection of differential alternative splicing from RNA-Seq data. *Nucleic Acids Res* **40**:e61. doi:10.1093/nar/gkr1291

Shiba T, Koga H, Shin H-W, Kawasaki M, Kato R, Nakayama K, Wakatsuki S. 2006. Structural basis for Rab11-dependent membrane recruitment of a family of Rab11-interacting protein 3 (FIP3)/Arfophilin-1. *Proc Natl Acad Sci* **103**:15416–15421. doi:10.1073/pnas.0605357103

Shinde MY, Sidoli S, Kulej K, Mallory MJ, Radens CM, Reicherter AL, Myers RL, Barash Y, Lynch KW, Garcia BA, Klein PS. 2017. Phosphoproteomics reveals that glycogen synthase kinase-3 phosphorylates multiple splicing factors and is associated with alternative splicing. *J Biol Chem* **292**:18240–18255. doi:10.1074/jbc.M117.813527

Shwetha S, Kumar A, Mullick R, Vasudevan D, Mukherjee N, Das S. 2015. HuR Displaces Polypyrimidine Tract Binding Protein To Facilitate La Binding to the 3' Untranslated Region and Enhances Hepatitis C Virus Replication. *J Virol* **89**:11356–71. doi:10.1128/JVI.01714-15

Thompson MG, Muñoz-Moreno R, Bhat P, Roytenberg R, Lindberg J, Gazzara MR, Mallory MJ, Zhang K, García-Sastre A, Fontoura BMA, Lynch KW. 2018. Co-regulatory activity of hnRNP K and NS1-BP in influenza and human mRNA splicing. *Nat Commun* **9**:2407. doi:10.1038/s41467-018-04779-4

Tsai P-L, Chiou N-T, Kuss S, García-Sastre A, Lynch KW, Fontoura BMA, Garcia-Sastre A, Lynch KW, Fontoura BMA. 2013. Cellular RNA binding proteins NS1-BP and hnRNP K regulate influenza A virus RNA splicing. *PLoS Pathog* **9**:e1003460. doi:10.1371/journal.ppat.1003460

Uzor S, Zorzou P, Bowler E, Porazinski S, Wilson I, Ladomery M. 2018. Autoregulation of the human splice factor kinase CLK1 through exon skipping and intron retention.

Gene **670**:46–54. doi:10.1016/J.GENE.2018.05.095

Vale-Costa S, Alenquer M, Sousa AL, Kellen B, Ramalho J, Tranfield EM, Amorim MJ. 2016. Influenza A virus ribonucleoproteins modulate host recycling by competing with Rab11 effectors. *J Cell Sci* **129**:1697–1710. doi:10.1242/jcs.188409

Vaquero-Garcia J, Barrera A, Gazzara MR, González-Vallinas J, Lahens NF, Hogenesch JB, Lynch KW, Barash Y. 2016. A new view of transcriptome complexity and regulation through the lens of local splicing variations. *Elife* **5**:e11752. doi:10.7554/eLife.11752

Venables JP, Koh C-S, Froehlich U, Lapointe E, Couture S, Inkel L, Bramard A, Paquet ER, Watier V, Durand M, Lucier J-F, Gervais-Bird J, Tremblay K, Prinos P, Klinck R, Elela SA, Chabot B. 2008. Multiple and specific mRNA processing targets for the major human hnRNP proteins. *Mol Cell Biol* **28**:6033–6043. doi:10.1128/MCB.00726-08

WHO | Influenza (Seasonal). 2019. . *WHO*. https://www.who.int/en/news-room/fact-sheets/detail/influenza-(seasonal)

Zhao N, Sebastiano V, Moshkina N, Mena N, Hultquist J, Jimenez-Morales D, Ma Y, Rialdi A, Albrecht R, Fenouil R, Sánchez-Aparicio MT, Ayllon J, Ravisankar S, Haddad B, Ho JSY, Low D, Jin J, Yurchenko V, Prinjha RK, Tarakhovsky A, Squatrito M, Pinto D, Allette K, Byun M, Smith ML, Sebra R, Guccione E, Tumpey T, Krogan N, Greenbaum B, van Bakel H, García-Sastre A, Marazzi I. 2018. Influenza virus infection causes global RNAPII termination defects. *Nat Struct Mol Biol* **25**:885–893. doi:10.1038/s41594-018-0124-7

Zu M, Li C, Fang J-S, Lian W-W, Liu A-L, Zheng L-S, Du G-H. 2015. Drug Discovery of

Host CLK1 Inhibitors for Influenza Treatment. *Molecules* **20**:19735–19747.

doi:10.3390/molecules201119653

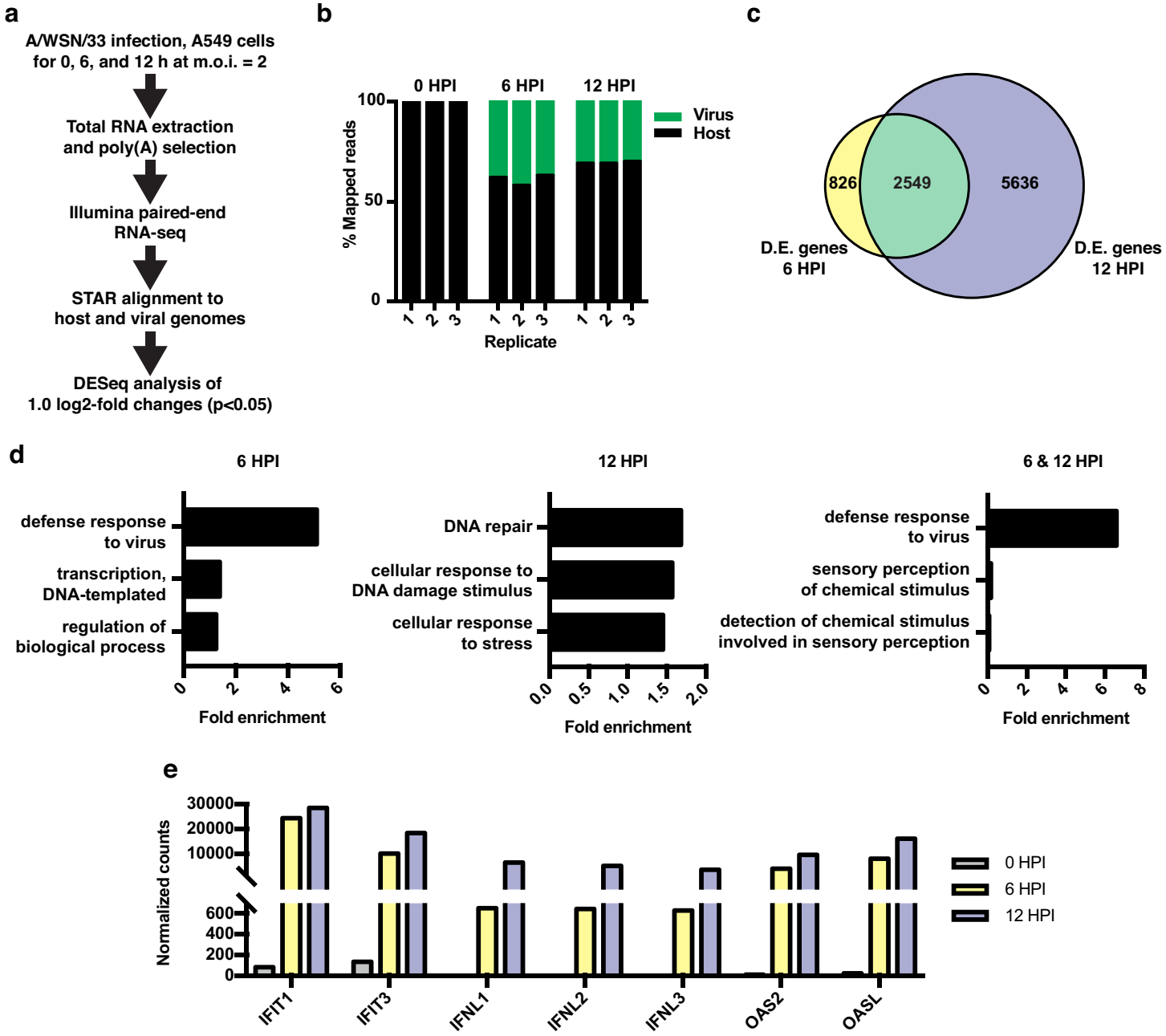

Figure 1. RNA-seq and differential expression analyses of IAV infected A549 cells. **(a)** Schematic of infections, RNA-seq, and data processing work-flow. **(b)** Proportion of aligned, mapped reads corresponding to host (hg19) and virus (A/WSN/33) in each of the indicated samples. **(c)** Overlap of differentially expressed genes with a log2-fold change > 1.0 at 6 and 12 h PI. **(d)** Top gene ontology categories for differentially expressed genes enriched at 6 h PI (left), 12 h PI (middle), and overlap of 6 and 12 h PI (right). P-values were <0.05 in all categories. **(e)** Normalized counts of known viral responsive genes.

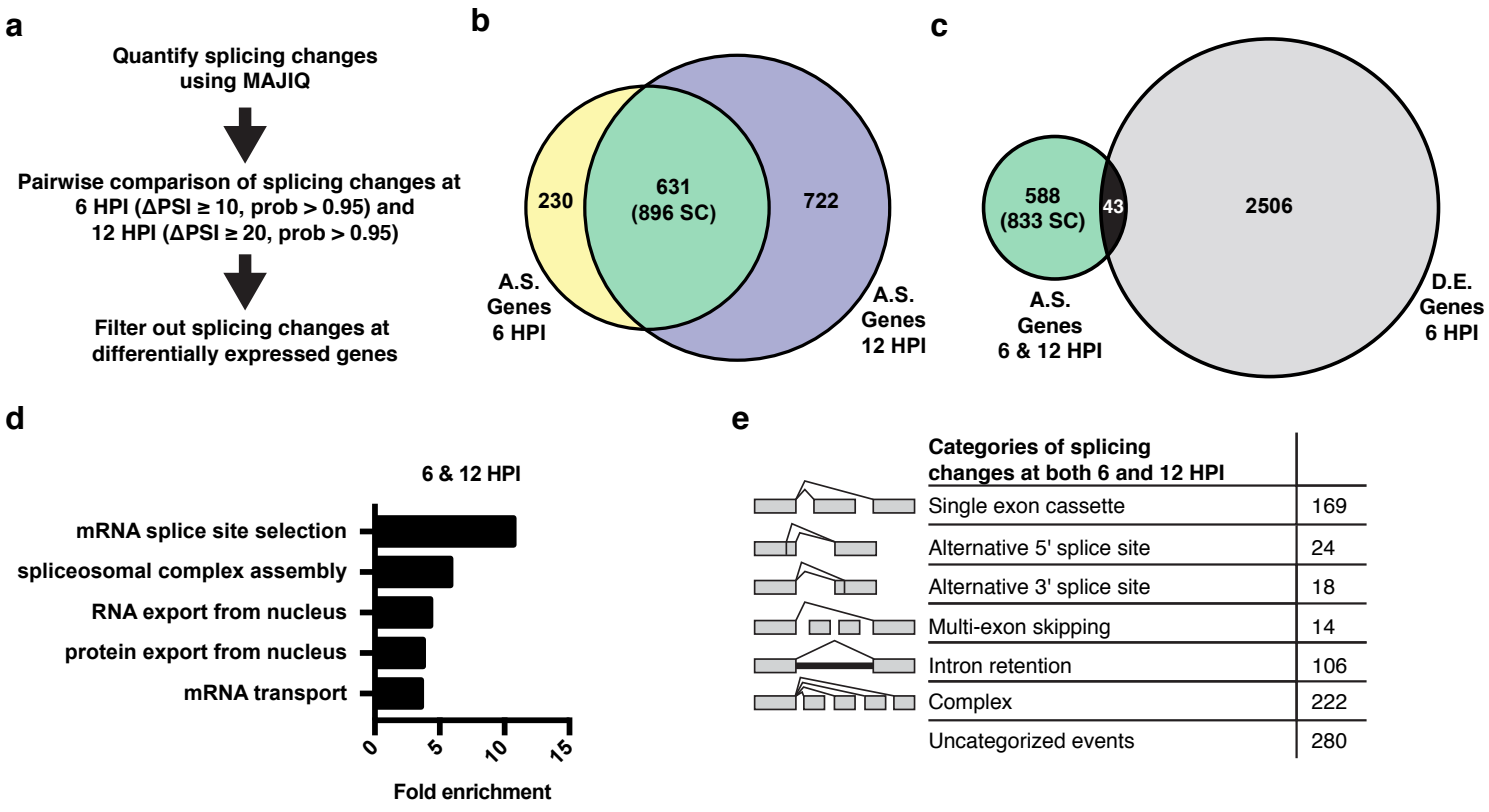

Categories of splicing changes at both 6 and 12 HPI	
Single exon cassette	169
Alternative 5' splice site	24
Alternative 3' splice site	18
Multi-exon skipping	14
Intron retention	106
Complex	222
Uncategorized events	280

Figure 2. Alternative splicing analyses of host genes during IAV infection. (a) Schematic of splicing analyses and downstream processing pipeline. **(b)** Overlap of alternatively spliced genes (ΔPSI ≥ 10 at 6 HPI (hours post-infection), ΔPSI ≥ 20 at 12 HPI) at 6 and 12 HPI (number of unique splicing changes (SC) shown in parentheses). **(c)** Overlap of alternatively spliced and differentially expressed genes at 6 and 12 HPI (number of unique splicing changes (SC) shown in parentheses, log2 fold-change > 1.0). **(d)** Top gene ontology categories enriched within 588 exclusively alternatively spliced genes at 6 and 12 HPI. P-values were <0.05 in all categories. **(e)** Categorization of 833 exclusively alternative splicing events (588 genes) at 6 and 12 HPI.

a

ABCD4	AGAP3	ARHGAP12	ARL14EP	ASB1	ASXL1	B4GALT3	C1orf52	CBX4
CCNT2	CHD2	CLASP1	CLK1	CREB1	DNAJB6	ECHDC2	EIF4A2	EIF4H
ENTHD2	EPC1	ERI2	FAM189B	FBXO22	GPBP1	GRAMD1A	HEATR3	IP6K2
IQCB1	KMT2D	LDLR	MANBA	MGAT5B	MTCL1	NCOR2	NR1D2	PALLD
PANK1	PAXBP1	PDE8A	PEX1	POM121	PPIP5K2	PTHLH	RAB11FIP3	RASA2
REPIN1	RIPK4	RWDD3	SETD5	SETX	SLC25A36	SMEK1	SNX4	STRN3
SUN1	TMEM256	TNRC6A	TRIM11	TSEN54	VEZF1	YTHDF1		

b

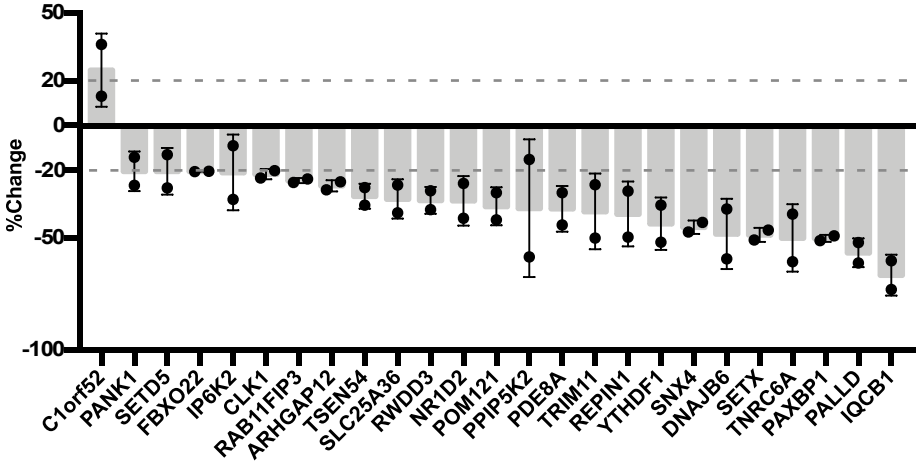

d

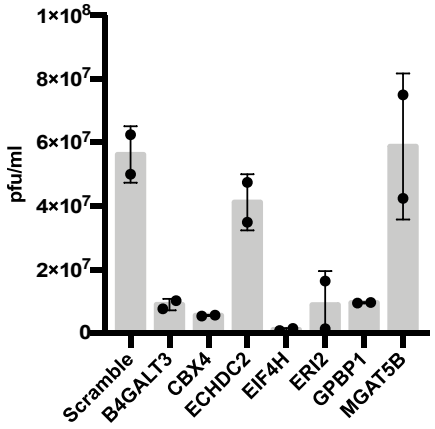

c

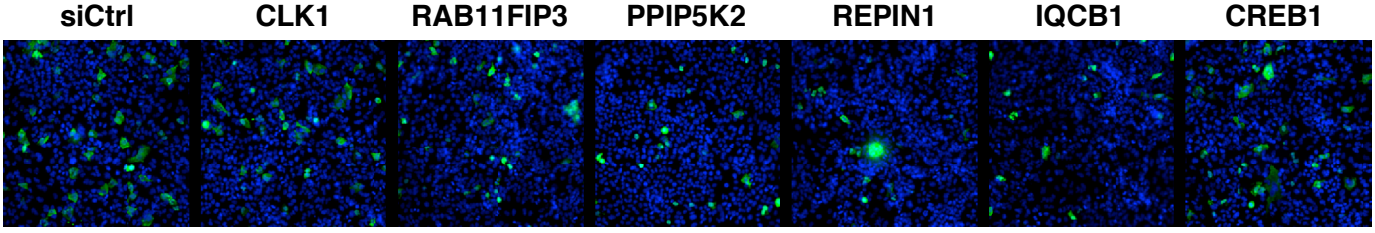

Figure 3. IAV-sensitive splicing events encode genes that modulate IAV replication.

(a) List of 61 alternatively spliced genes sensitive to IAV infection chosen for siRNA screening. **(b)** Percent change of IAV positive scoring cells in the context of siRNA knockdown. Bar indicates the average of two independent screens, dots and error bars represent individual data points. Genes with an average change of ≥20% are plotted. **(c)** Representative images of immunofluorescence imaging of IAV infected cells in the context of control or gene targeting siRNA treatments. Blue staining denotes individual nuclei (DAPI) and green staining denotes IAV positive cells (NP). **(d)** A549 cells were treated with 20 nM siRNA for 72 hours and infected with IAV at moi = 0.01 for 48 hours. Shown is the measurement of plaque forming units in media via plaque assay. Bar indicates the average of two independent screens, dots and error bars represent individual data points.

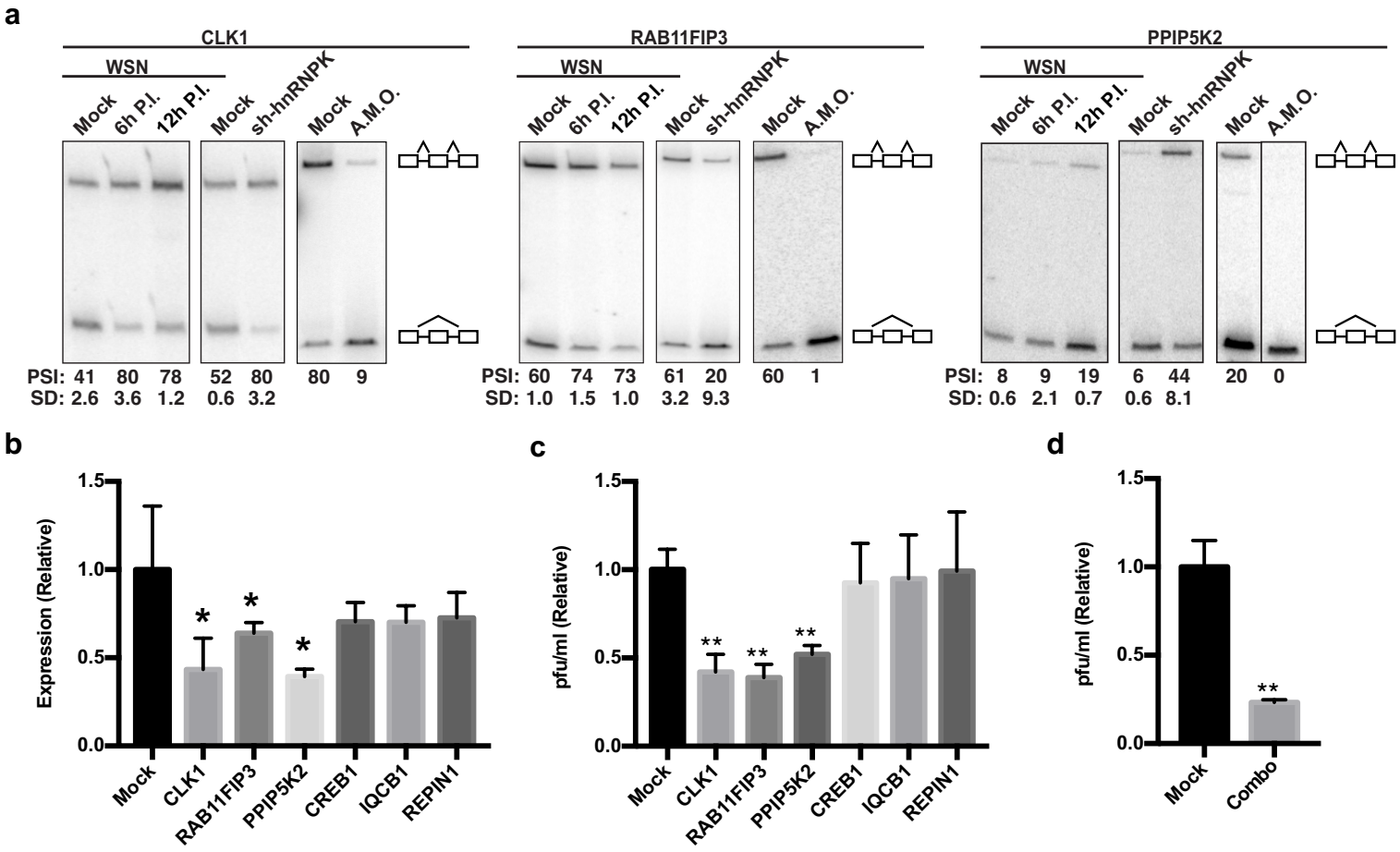

Figure 4. Altering splicing of host genes results in IAV replication changes. (a) A549 cells were infected (WSN), treated with shRNA against hnRNP K, or treated with splice-blocking antisense morpholino oligonucleotides (AMOs). Splicing was analyzed using RT-PCR analyses (additional gels in Fig. S3a) **(b)** RT-qPCR analyses (values normalized to mock AMO treatment) of PA segment vRNA 48 HPI with IAV (moi = 0.01) in the context of AMO treatment (targeted genes indicated on x-axis). Values are means ± s.d. from three independent experiments. **(c)** Measurement of plaque forming units (values normalized to mock AMO treatment) in media 48 HPI with IAV WSN (moi = 0.01) in the context of AMO treatment (targeted genes are indicated on x-axis). Values are means ± s.d. from three independent experiments. **(d)** Measurement of plaque forming units (values normalized to mock AMO treatment) in media 48 HPI with IAV WSN (moi = 0.01) in the context of AMO treatment. In combo treated cells CLK1, RAB11FIP3, and PPIP5K2 were simultaneously targeted with AMO's. Values are means ± s.d. from three independent experiments. Statistical significance was determined via two-tailed student's t-test where $p<0.05$ = * and $p<0.005$ = ** when comparing mock AMO treatments vs AMO treated samples.

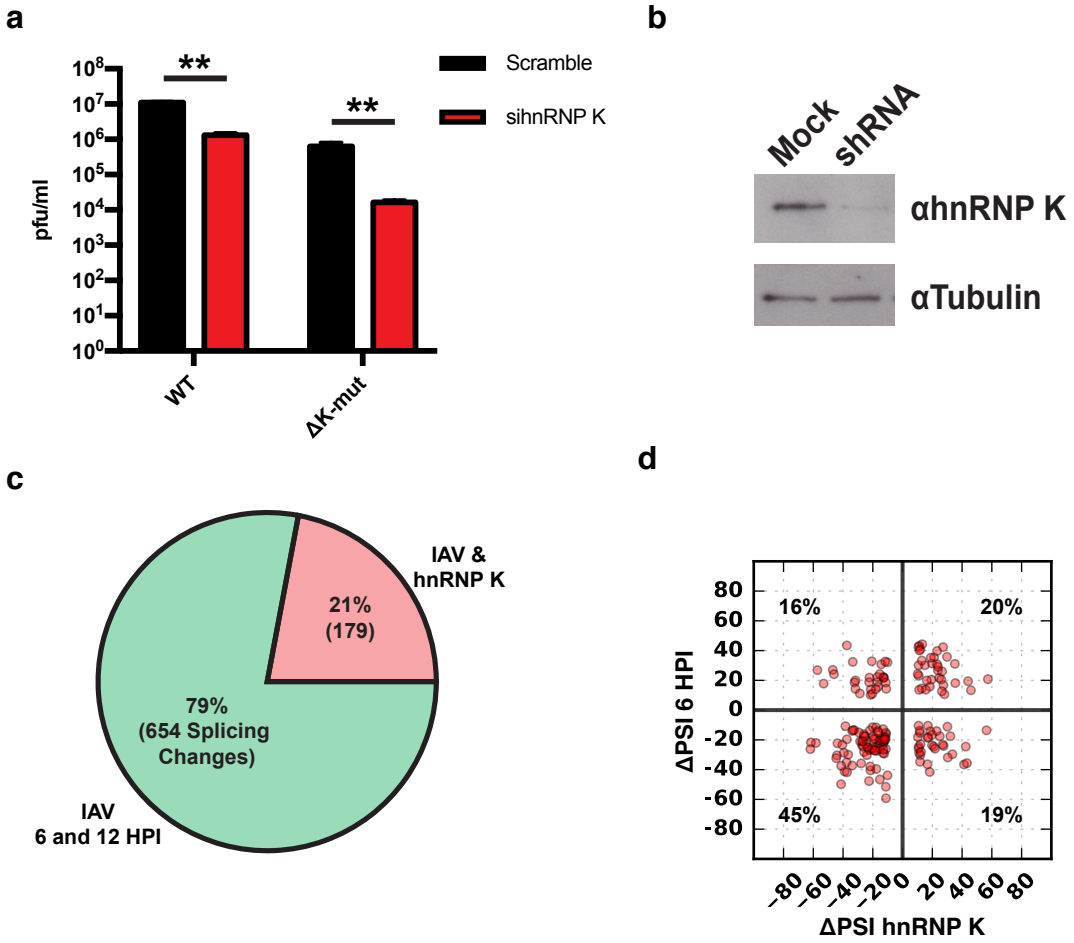

Figure 5. hnRNP K regulates a subset of IAV-induced splicing events during infection. (a) A549 cells were infected with WT and ΔK-mut IAV in the context of scrambled or hnRNP K targeting siRNA. Plaque forming units in media were assayed at 48 HPI. Values are means ± s.d. from three independent experiments. $p<0.005$ = **. Statistical significance was determined via two-tailed student's t-test where $p<0.05$ = * and $p<0.005$ = ** when comparing scramble vs siRNA treated samples. **(b)** Western blot of shRNA treated cells. Tubulin is shown as a loading control. **(c)** Proportion of IAV sensitive splicing events (observed at 6 and 12 HPI) that are also sensitive to hnRNP K knockdown. **(d)** ΔPSI value comparison of 179 splicing events at 6 HPI or after hnRNP K knockdown. Percentage values denotes proportion of 179 splicing events residing in each quadrant.

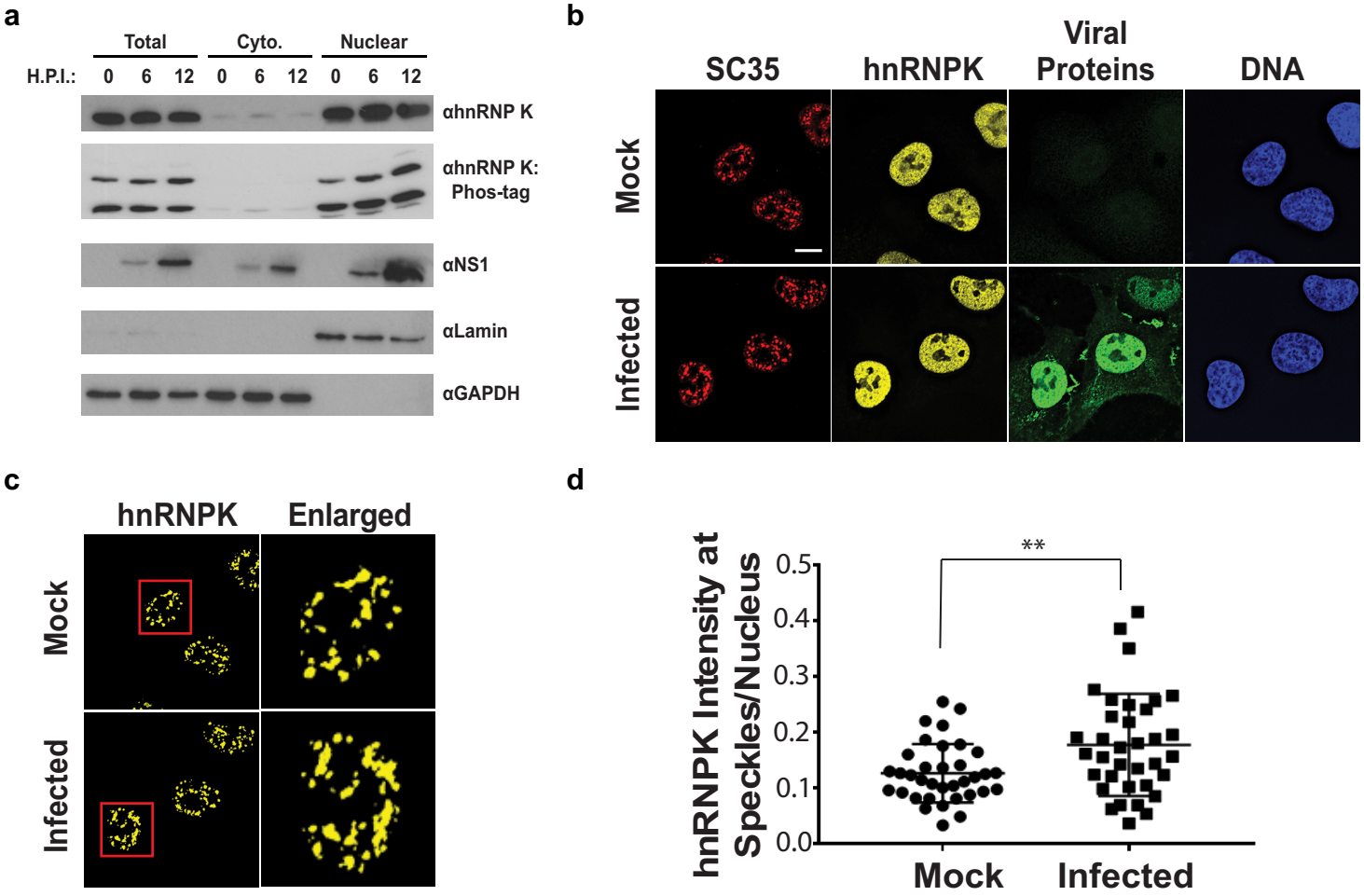

Figure 6. hnRNP K levels increase at nuclear speckles during influenza A virus infection. (a) Western blot analyses of total, cytoplasmic, or nuclear A549 cell extracts 0, 6, and 12 hours post infection (HPI). hnRNP K was analysed via traditional SDS-PAGE or Phos-tag to separate phosphorylated isoforms of hnRNP K. **(b)** Approximately 100% of A549 cells were infected with influenza virus (WSN) for 5 h and then subjected to immunofluorescence microscopy to detect SC35, hnRNP K, and viral proteins. Nuclear speckles were marked with anti-SC35 antibody. Scale bar = 10μm. (**c)** Voxel outside surface generated for nuclear speckles was set to 0 for hnRNP K channel to visualise hnRNP K at nuclear speckles. The marked region is enlarged. **(d)** Quantification of hnRNP K at nuclear speckles was performed using the Imaris software. hnRNP K intensity sum at nuclear speckles was normalized to the intensity sum in the nucleus. Values are means ± s.d. measured in 35 mock and 35 WSN infected cells from biological triplicates. **t-test $P<0.01$.

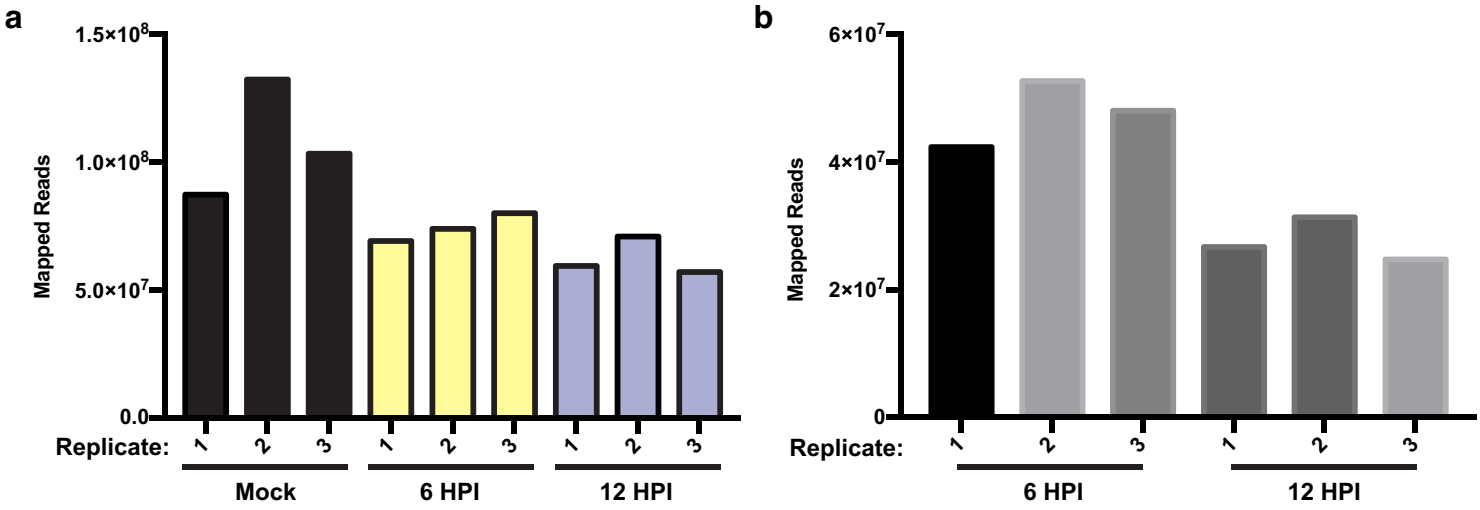

Figure S1. (a) Unique RNA-seq reads mapped to human genome in mock, 6 h, and 12 h IAV infections in A549 cells across 3 replicates. **(b)** Unique RNA-seq reads mapped to A/WSN/133 reference genome at 6 and 12 HPI in A549 cells across 3 replicates

Thompson et al_ Fig S2

a

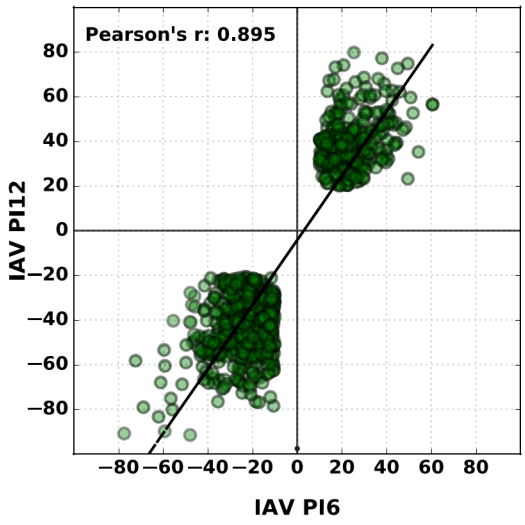

b

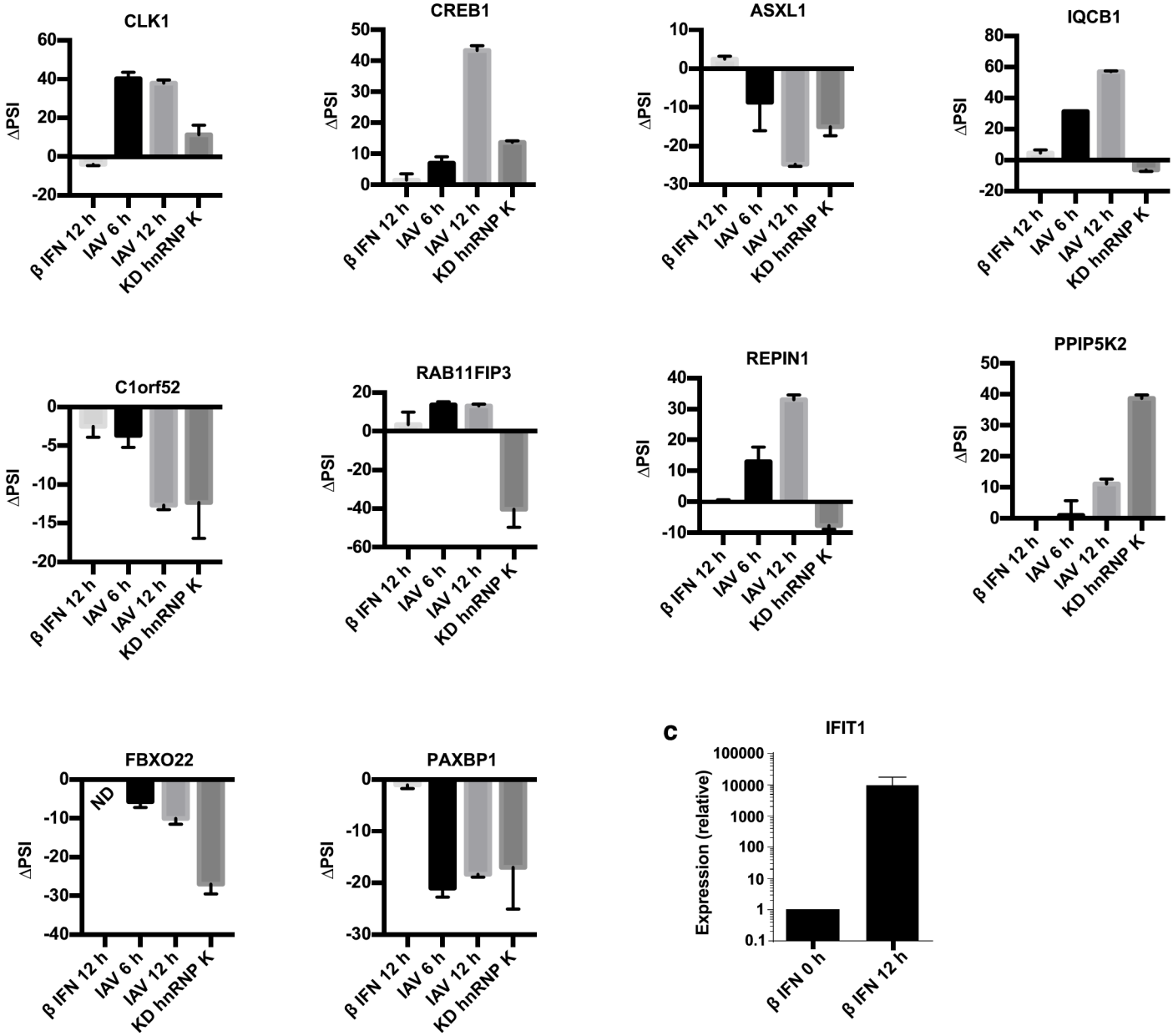

c

Figure S2. (a) Percent change in splicing values at 6 and 12 HPI vs. mock, for the 896 splicing events that are persistently changed upon viral infection (see Fig. 2b). **(b)** A549 cells were treated with interferon beta (IFNβ), infected with virus (WSN), or treated with shRNA against hnRNP K. Splicing was quantified using radioactive RT-PCR. ΔPSI values were determined by subtracting percent-exon-included in mock conditions from experimental conditions. Values are means ± s.d. from 2-3 biologically independent experiments. **(c)** Quantification of interferon inducible gene IFIT1 relative to Actin, by qPCR, in samples from panel b.

a

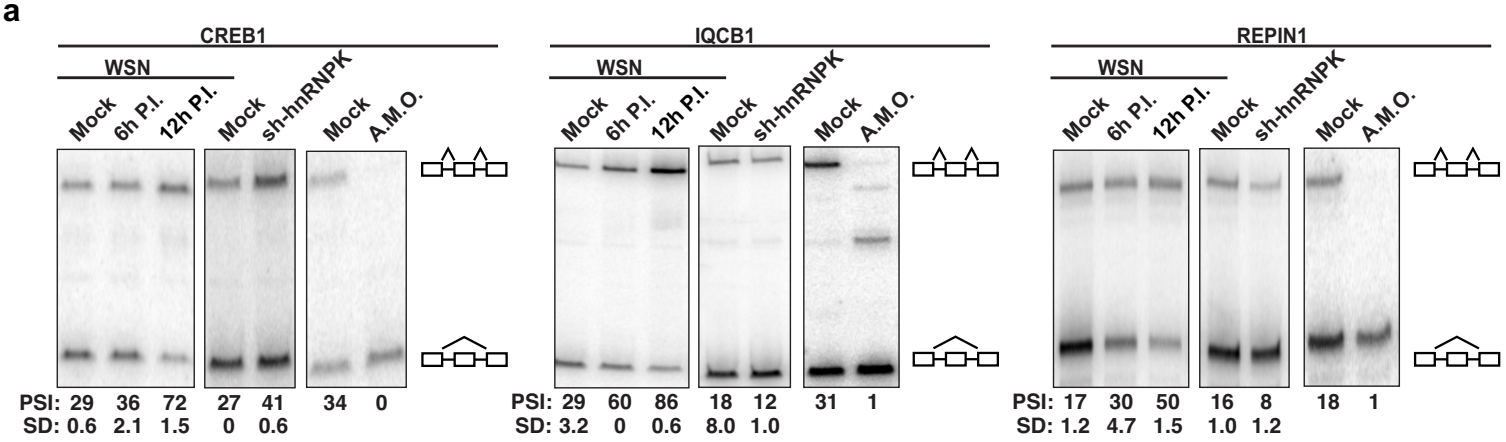

b

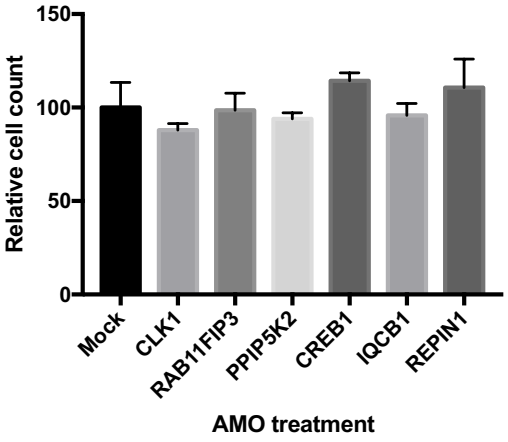

Figure S3. (a) A549 cells were infected (WSN), treated with shRNA against hnRNP K, or treated with splice-blocking antisense morpholino oligonucleotides (AMOs). Splicing was analyzed using RT-PCR analyses **(b)** Normalized cell counts of mock or AMO treated A549 cells (values normalized to mock AMO treated cells)

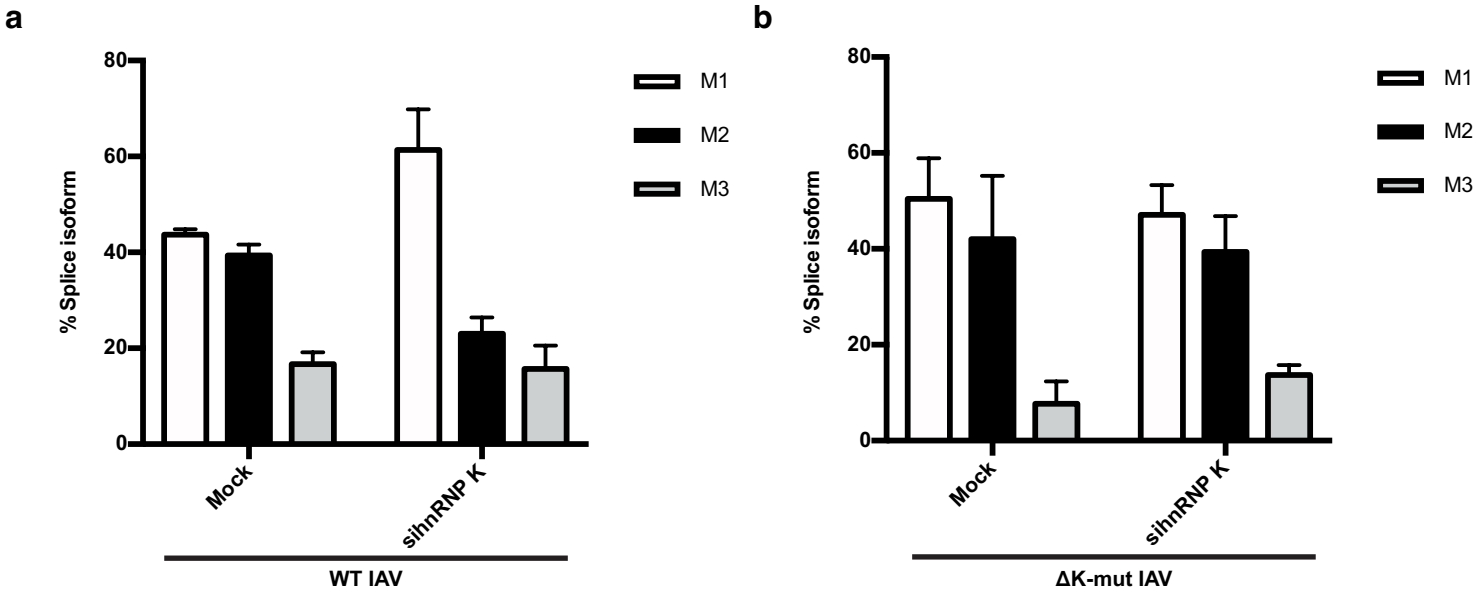

Figure S4. (a) Quantification of M segment isoform levels in A549 cells infected with WT IAV in the context of scrambled or hnRNP K targeting siRNA using radioactive primer extension and densitometry. **(b)** Quantification of M segment isoform levels in A549 cells infected with ΔK-mut IAV in the context of scrambled or hnRNP K targeting siRNA using radioactive primer extension and densitometry. Values are means ± s.d. from three biologically independent experiments.